Composites Part A 113 (2018) 132–140

Contents lists available at ScienceDirect

Composites Part A

journal homepage: www.elsevier.com/locate/compositesa

Research on high electromagnetic interference shielding effectiveness of a foldable buckypaper/polyacrylonitrile composite film via interface reinforcing

Qianshan Xia[a], Zhichun Zhang[a], Hetao Chu[a], Yanju Liu[b], Jinsong Leng[a,*]

[a] Center for Composite Materials and Structures, No. 2 YiKuang Street, Science Park of Harbin Institute of Technology (HIT), Harbin 150080, PR China
[b] Department of Aerospace Science and Mechanics, No. 92 West DaZhi Street, Harbin Institute of Technology (HIT), Harbin 150001, PR China

ARTICLE INFO

Keywords:
Buckypaper
Polymer-matrix composites
Electromagnetic interference shielding

ABSTRACT

Herein, a series of foldable buckypaper/polyacrylonitrile (BP/PAN) composite films were developed in a facile strategy. This strategy was based on electrospun and vacuum pressurized filtration methods. The composite film had better mechanical properties than pristine BP via interface reinforcing, but not deprived of excellent conductivity. The maximum tensile strength and elongation at break of BP/PAN films were 1.45 and 11.65 times than pristine BP, respectively. Moreover, BP/PAN film had higher electromagnetic interference (EMI) shielding effectiveness (63.7–65 dB) in the Ku band (12–18 GHz) than pristine BP (34.3–42.9 dB), due to interfaces forming between PAN fibers and CNTs. The BP/PAN composite as a promising EMI shielding material could be utilized in military and civil applications, such as flexible antenna, EMI shielding clothes and soft portable electronic products.

1. Introduction

With the rapid development of information and communications technology, advanced electrical and electronic devices have played dominant roles in various fields. However, electromagnetic radiation pollution, which comes from commercial and military telecommunication equipment, not only leads degradation of the device performance, but also harms humans' health [1]. The severe pollution of electromagnetic (EM) wave radiation has attracted more and more researchers' attention [2]. It is urgent to isolate precision instrument and mankind from electromagnetic wave radiation. In order to achieve the goal, researchers show an intense interest in preparation of ideal electromagnetic interference (EMI) shielding materials.

At first, metals and metal oxides had been used as traditional EMI shielding materials, such as Fe [3], Al [4], Cu [5], Fe_3O_4 [6], etc. [7,8], based on high conductivity or magnetic loss. However, their application fields were severely limited by many fatal factors that contained high density, easy corrosion, poor flexibility [9]. In addition, metal and metal oxide/polymer composites were also extensively studied. When flexible and light-weight materials were required in some specific conditions, these composites were not suitable [10]. Therefore, corrosion-resistant, flexible and lightweight materials have also been considered in EMI shielding field.

In recent decades, carbon materials [11–15] and their composites [16,17], owing to their low density, anti-corrosion, excellent electrical and thermal properties [18], play important roles in development of shielding materials. The one-dimensional cylindric carbon nanotube (CNT) was first found in 1991 [19]. Since then more and more researches on CNT and its composites with outstanding electrical properties, corrosion resistance and low density have been widely reported. Carbon nanotube film as a macro-material of CNT, which is also called 'Buckypaper', has potential applications in the thermally and electrically conductive material fields, such as anti-icing [20], EMI shielding [21], lightning striking protection [22], electrodes of lithium battery and super capacitor [23,24]. At present, buckypaper (BP) has been mainly manufactured via chemical vapor desposition [25] (CVD) or vacuum based and pressurized filtration [26] methods. Nevertheless, the high friability and poor mechanical properties restrict its application in engineering. To overcome shortcomings of BP, two main strategies have been focused on, including preparations of cross-linked BP and BP/polymer composites. Typically, the reaction between functional CNTs and cross-linking agent changes the intertube interaction from weaker Van der Waals force to stronger chemical bonding for improving mechanical properties of BP [27]. However, chemical functionalization could damage the intrinsic structure of CNT, so that electrical conductivity of BP is reduced. Although BP/polymer matrix

* Corresponding author.
E-mail address: lengjs@hit.edu.cn (J. Leng).

https://doi.org/10.1016/j.compositesa.2018.07.019
Received 8 March 2018; Received in revised form 12 July 2018; Accepted 15 July 2018
Available online 17 July 2018
1359-835X/

composites hold better mechanical properties, lower pliability and electrical conductivity are inevitably gotten [28]. It could be interpreted that BP is coated by insulating and rigid polymers.

For overcoming above drawbacks, an EMI shielding material that balances flexibility and conductivity is urgently demanded. The electromagnetic shielding fabric materials with better flexibility could be manufactured as shielding clothes, shielding tents and other flexible EMI layers, to ensure security of health and information [29]. In this study, a novel lightweight and foldable BP/PAN composite film with ultra-high EMI shielding efficiency was made via electrospun and vacuum pressurized filtration methods. Meanwhile, EMI shielding properties of composite films with various CNT contents were characterized in the Ku-band frequency range (12–18 GHz). The Ku-band was the electromagnetic waveband for satellite communication and civil aviation. Compared with pristine BP, the mechanical and EMI shielding properties of BP/PAN films were obviously enhanced by interface reinforcing between the CNTs and PAN fibers. Therefore, reinforcement mechanisms for mechanical and EMI shielding properties of BP/PAN composite film were explained in this paper, to highlight the superiority of its unique structure.

2. Experimental

2.1. Materials

The single-walled carbon nanotubes (SWCNTs) whose product model was TNSR were provided by Chengdu Organic Chemicals Company Limited. To obtain highly dispersed SWCNT solution, the sodium dodecyl sulfate (SDS, analytical reagent) was supplied by Aladdin Chemical Reagent Co., Ltd. and used as the surface-active agent. Deionized (DI) water was home-made. The polyacrylonitrile (PAN) powders were purchased from Sigma-Aldrich and the average molecular weight was 150,000 g/mol. The N,N-dimethylformamide (DMF) was obtained from Tianjin Fengchuan Chemical Reagent Technologies Co., Ltd. and its content was more than 99.5%. Without further purification, all the chemicals were used as received.

2.2. Methods

2.2.1. Preparation of PAN electrospun mats

According to our previous report [30], a certain amount of PAN powders was stirred in DMF for 5 h at room temperature until the powders were completely dissolved. Then the solution was placed in a cylinder containing the active electrode that was parallel to the collecting electrode in the “NanospiderTM” electrospinning equipment [31]. The optimized parameters used in the electrospinning experiment were room temperature, humidity of 33% and a driving voltage of 45 kV, respectively. The distance between active and collecting electrodes was 20 cm and the rotation speed of the active electrode was 1 r/min. Subsequently, the electrospun film was received on an aluminum foil through PAN microfiber accumulating. To remove the residual DMF, the PAN film was peeled from aluminum foil and placed in an air-circulating oven at 50 °C for 10 h. Then 5 L DI water was infiltrated through an as-prepared PAN mat that was covered on a Büchner funnel. After infiltrating and washing by DI water 5 times, the wet PAN mat was dried in an oven for 5 h at 90 °C and measured by a micrometer. The sizes of PAN mats were about 300 × 430 × (0.06 ± 0.005) mm^3 and their areal density was about 3 mg/cm^2. All these mats were cut into 140 × 140 × (0.06 ± 0.005) mm^3 for preparing the BP/PAN composite films.

2.2.2. Preparation of SWCNT suspension

To attain homogeneous CNT suspension, 1–5 g SDS was completely dissolved into 5 L DI water by mechanical stirring for 1 h. Subsequently, 0.2–1 g SWCNTs were added into the SDS solution and continued to stir for 2 h. Then, the mixture underwent circulation and ultrasonic dispersion twice by a high-power ultrasonic processor, to obtain a homogeneous suspension solution according to our previous report [32].

2.2.3. Fabrication of self-assembly BP

BP with areal density of 3 mg/cm^2 was prepared in this work as a control sample. Firstly, a certain volume of CNT suspension was infiltrated through a nylon filter membrane with pore size of 0.45 um that was covered on a Büchner funnel. After infiltrating and washing by DI water 5 times, the wet BP was dried in an oven for 5 h at 90 °C and peeled from the filter membrane. Then, the as-prepared BP was cut into size of 140 × 140 × 0.04 mm^3 and designated as 3#BP.

2.2.4. Fabrication of self-assembly BP/PAN composite films

In this study, BP/PAN composite films with various CNT areal densities were prepared by controlling the volume and concentration of CNT suspension, namely, 1 mg/cm^2, 2 mg/cm^2, 3 mg/cm^2 and 4 mg/cm^2. Firstly, the homogeneous SWCNT suspension was infiltrated into a PAN electrospinning film that was covered on the top surface of Büchner funnel, to form BP/PAN composite film. Then all the wet BP/PAN films were washed 5 times by DI water and dried at 90 °C for 24 h. The 1–4 mg/cm^2 composite films with size of 140 × 140 × (0.07/0.09/0.11/0.13) mm^3 were designated as 1#, 2#, 3# and 4#BP/PAN respectively. The fabrication process of BP/PAN composite film was displayed in Fig. 1.

2.3. Characterization

Scanning electron microscopy (SEM) observations were carried out via a Focused Ion Beam/Scanning Electron Microscope (FEI HELIOS NanoLab 600i) and operated at a voltage of 30 kV. Nitrogen adsorption isotherm measurement was analyzed by a volumetric adsorption analyzer (Micrometrics ASAP 2020), and surface and pore features of samples were calculated by Barrett-Emmett-Teller (BET) method. Mechanical properties of all the samples at room temperature were tested through a static stretching module of the TA Q800 Dynamic Mechanical Thermal Analysis (DMTA), with force loading from 0.001 to 18 N and tensile speed of 0.5 N/min [33]. All the tensile specimens were cut into the rectangle shape (20 × 2 mm^2) and every five ones were selected from BP, PAN and 1-4#BP/PAN films, respectively. And, all the samples were statically pulled until they were ruptured without heating, and the average values of average tensile strength and elongation at break were gotten by calculating. Electrical resistivity of samples was studied by a manual four point probe sheet resistance/resistivity measurement system (Napson RG-7C), and the results came from the average electrical resistivity of five test points in each sample. EMI shielding properties were recorded with an Agilent N5227A Vector Network Analyzer (VNA) and a waveguide tube (12–18 GHz). The samples with different thicknesses were cut into small pieces with dimensions of 15.8 × 7.9 mm^2 to fit the waveguide holder, and every three samples were selected from BP, PAN and 1-4#BP/PAN films, respectively. Total EMI shielding effectiveness (SE_{total}), reflection EMI shielding effectiveness (SE_R) and absorption EMI shielding effectiveness (SE_A) was determined on the basis of measured S parameters (S_{11}, S_{12}, S_{21} and S_{22}). We measured SE_{total} and SE_R in dB unit and their average values were gotten by calculating three samples.

3. Results and discussion

3.1. Morphology and microstructure characterization

The SEM micrographs that were displayed in Fig. 2 were the surfaces of BP layers of 1-4#BP/PAN films. Surfaces of BP layers clearly exhibited uneven and porous. Moreover, CNT networks were tightly constructed via CNT bundles randomly distributing. Compared with Fig. 2(a)–(d), pore diameters of CNT networks reduced with CNT

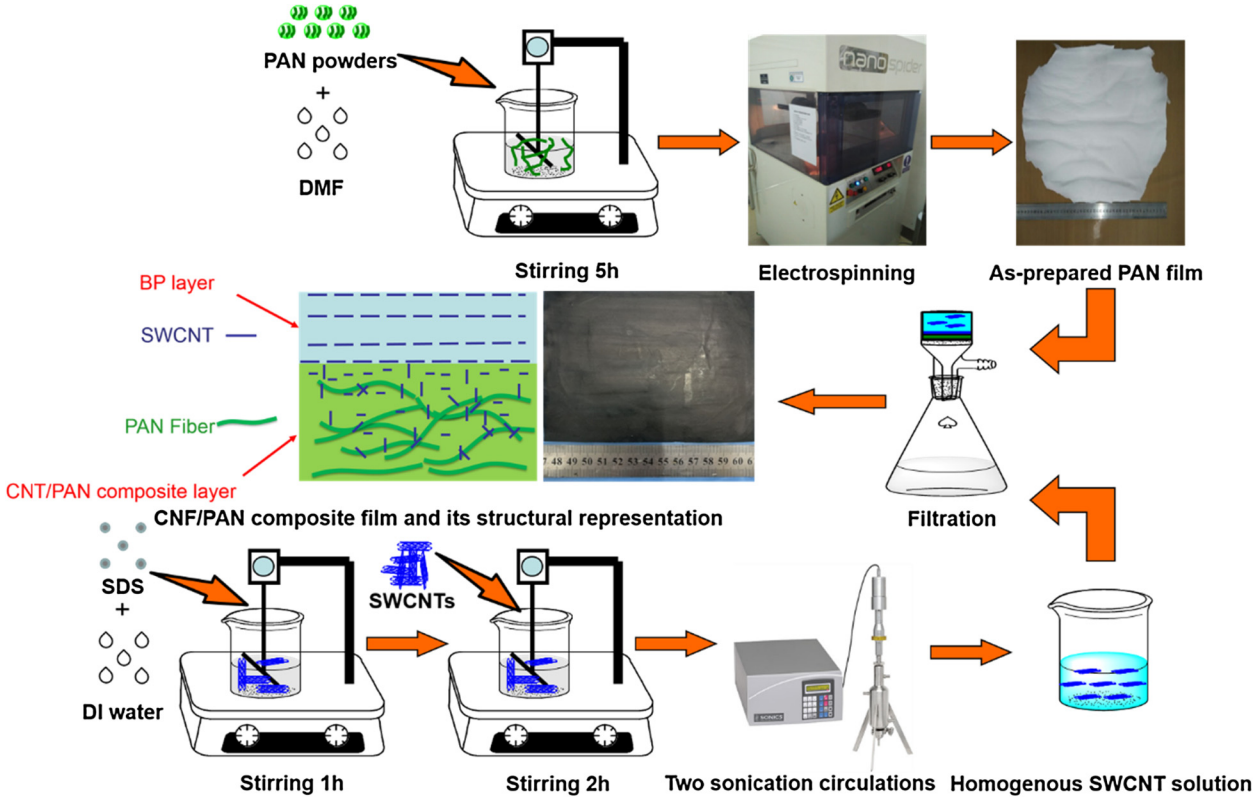

Fig. 1. The schematic representation of fabrication process of BP/PAN composite films. (For interpretation of the references to colour in this figure legend, the reader is referred to the web version of this article.)

content increasing and the CNT bundles turned to thicker with the concentration of CNT suspension increasing. One simple reason was the quantity of CNT increasing. Meanwhile, the physical cross link points between CNT bundles also increased, which obtained from Vander Waals forces and π-π interactions. As a result, thicker CNT bundles closely linking led the denser BP layers forming via self-assembly [32]. Therefore, the BP layer of BP/PAN film offered effective pathways for electron transport between CNT bundles, so that BP layer had excellent conductivity. It permitted BP layer of BP/PAN film to be manipulated as a reflective layer for EMI shielding.

Fig. 3(a–e) were surfaces of CNT/PAN layer of 1-4#BP/PAN composite films and pristine PAN mat at low and high magnification. The

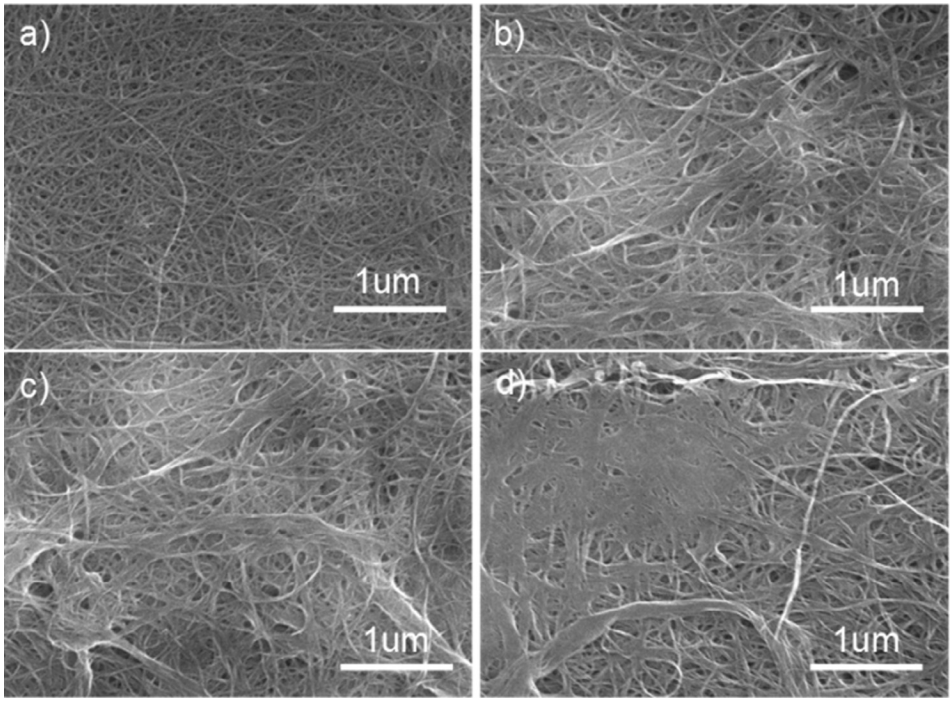

Fig. 2. (a), (b), (c) and (d) The porous BP layer surfaces of 1-4#BP/PAN composites.

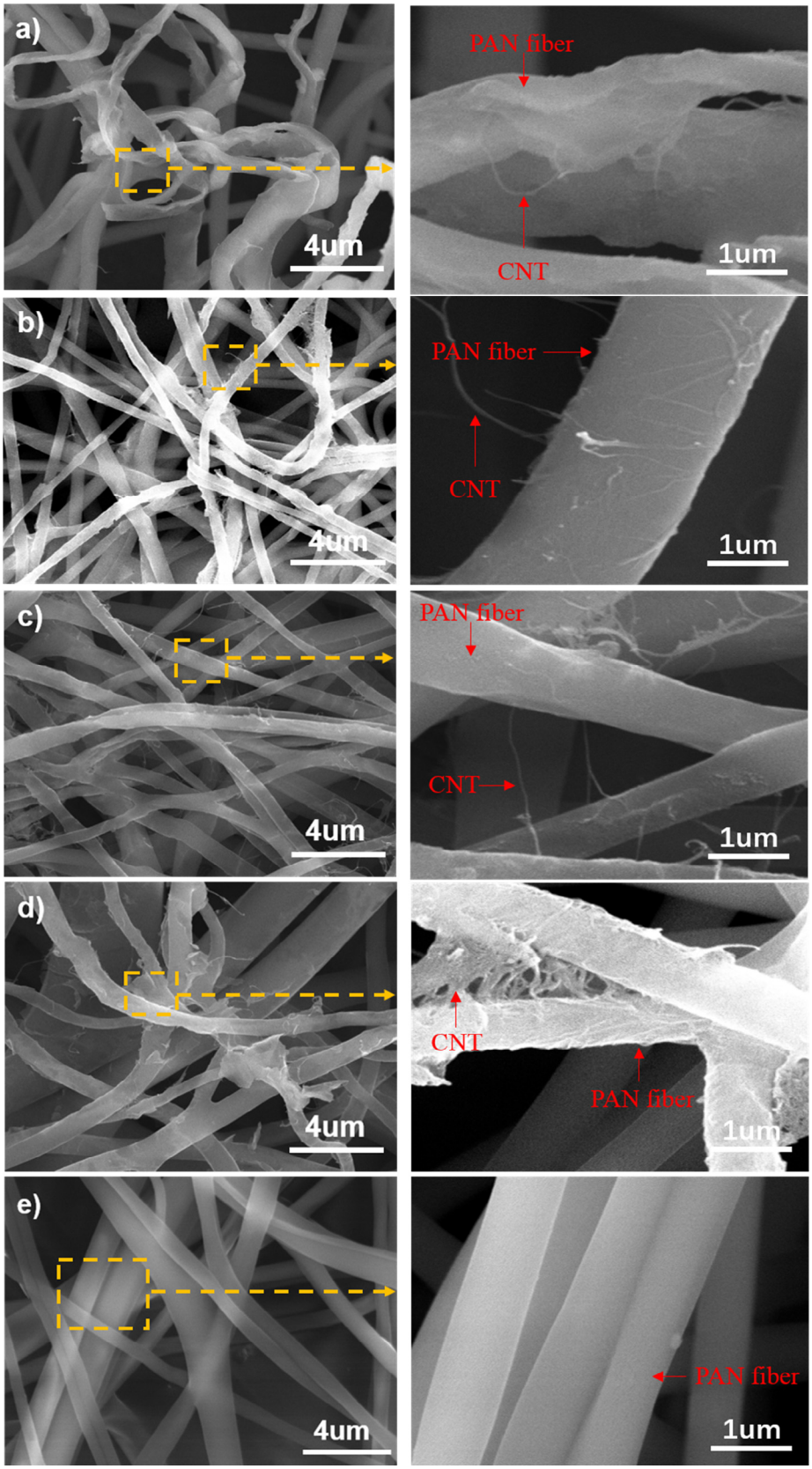

Fig. 3. (a), (b), (c), (d) and (e) The surfaces of CNT/PAN layer of 1-4#BP/PAN films and pristine PAN film at low and high magnification. (For interpretation of the references to colour in this figure legend, the reader is referred to the web version of this article.)

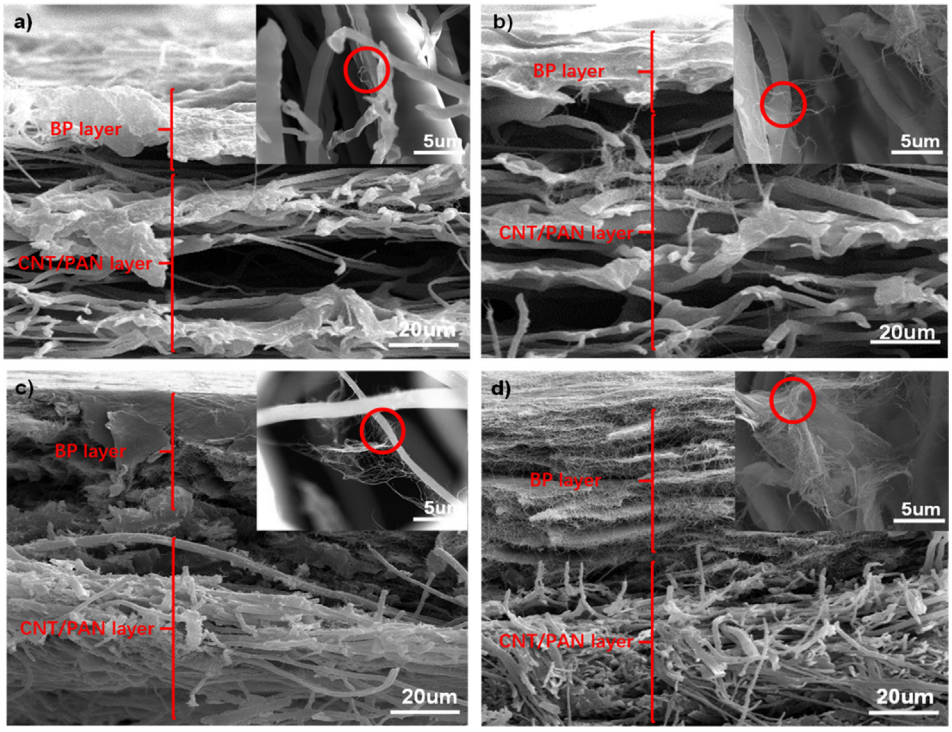

Fig. 4. (a), (b), (c) and (d) The cross profiles of 1-4#BP/PAN composite; the insert images were the partial enlargements. (For interpretation of the references to colour in this figure legend, the reader is referred to the web version of this article.)

surfaces of CNT/PAN layers of 1-4#BP/PAN films and pristine PAN mat contained a large sum of pores and the pore size was around 10 um. There were numerous cross-linking points between PAN fibers that came from electrostatic force. Moreover, all the PAN fibers exhibited smooth and uniform. The diameters were varied from 1 to 3 μm. There were some CNTs randomly twining on surfaces of PAN fibers in Fig. 3(a)–(d), thus it provided many interfaces for improving microwave absorbing ability of BP/PAN composite film [34–38]. Compared with Fig. 3(a–e), the CNT quantity that twined on PAN fibers increased with the increase of CNT areal density.

In addition, Fig. 4 showed the cross sections of 1-4#BP/PAN composite films after rupture, and the upper and lower sections were BP and CNT/PAN layers respectively. Thickness values of BP layers were about from 20 to 60 μm in Fig. 4. However, boundaries between BP and CNT/PAN layers were not obvious. Furthermore, both CNT distribution volumes in composites and penetration depth in CNT/PAN layers displayed an increase trend with CNT content increasing. On the other hand, PAN fibers were twined by CNTs as shown in the red circles and the quantity of twining CNTs also exhibited an increase trend with CNT areal density increasing in the insert images of Fig. 4(a)–(d). The diameters of PAN fibers were approximately 100 times thicker than the CNTs that twined on fibers. When microwave shot into CNT/PAN layer, more interfaces forming between PAN fibers and CNTs provided more chances to consuming power of electromagnetic wave [39,40]. Compared to pristine BP, it was a reasonable evidence that the CNT/PAN layer filled with CNTs as a microwave absorbing layer was beneficial for improvement on EMI shielding ability of BP/PAN composite.

As PAN fibers introduced, more interfaces formed in 3#BP/PAN composite film compared with pristine BP. Therefore, it was another way to investigate interfaces of composite through comparing with the differences of pore and surface features between 3#BP and 3#BP/PAN. The pore diameter distribution curves in Fig. 5 were obtained from the nitrogen dV/dlogD adsorption isotherms and calculated by the BET method. Obviously, pore diameter distribution ranges of 3#BP and 3#BP/PAN exhibited narrow and the mesopore structures in accordance with the International Union of Pure and Applied Chemistry's

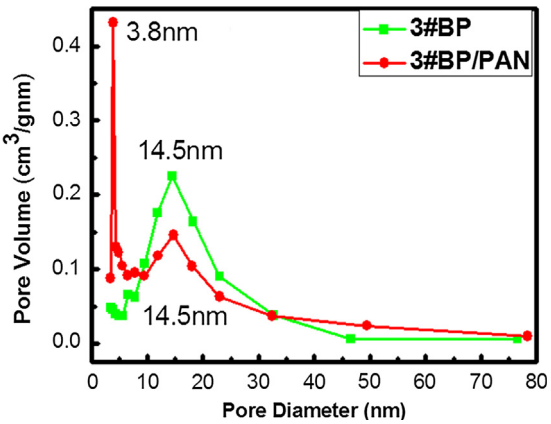

Fig. 5. Pore size distributions of 3#BP and 3#BP/PAN. (For interpretation of the references to colour in this figure legend, the reader is referred to the web version of this article.)

(IUPAC) [41]. Additionally, the largest pore volumes of 3#BP/PAN and 3#BP appeared at 3.8 nm and 14.5 nm respectively. Because the mesopore structure of BP was provided by empty space among CNT bundles and that of BP/PAN formed through CNT bundles, PAN fibers and interfaces between CNTs and PAN fibers overlapping.

3.2. Mechanical property analysis

Better mechanical properties of BP/PAN composite film were the key parameters to expand its application fields. The tensile strength and elongation at break of pristine PAN mat, 3#BP and 1-4#BP/PAN films were shown in Fig. 6. The insert photo was a paper boat that was made by 3#BP/PAN composite film. It indicated that the composite film could be folded as an ordinary paper. Compared with 1-4# composite films, there was little difference between their flexibility. It proved that CNT content had little effect on the flexibility of 1–4 mg/cm^2 BP/PAN

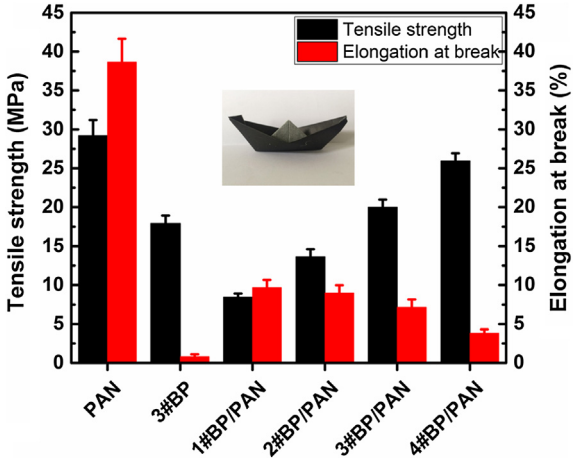

Fig. 6. Tensile strength and elongation at break of PAN mat, 3#BP and 1-4#BP/PAN composites; the inset image is a folding boat using the 3#BP/PAN film to display its flexibility and foldability. (For interpretation of the references to colour in this figure legend, the reader is referred to the web version of this article.)

composite films. The average tensile strength values of 1-4#BP/PAN films increased with CNT areal density increasing, which was ranged from 8.42 to 25.94 MPa, and the tensile strength of 4#BP/PAN film was the maximum value (25.94 MPa). Depending on Fig. 4, the fraction modes of both the BP layer and CNT/PAN layer were brittle rupture. Moreover, thickness values of CNT/PAN layers were same for all prepared BP/PAN films, and those of BP layers increased with the CNT areal density increase. It led to the interaction between CNTs increasing. Thus, the thicker thickness provided higher tensile strength for BP/PAN composite film. However, the average elongation at break values of 1-4#BP/PAN composites showed an opposite trend, and the maximum and minimum values were 9.67% (1#BP/PAN) and 3.82% (4#BP/PAN), respectively. Fig. 4 displayed thickness values of BP layers were increased with the CNT areal density increasing and the fraction modes of BP layers belonged to brittle rupture. Furthermore, tensile strength of BP layer was lower in Fig. 6. It caused BP layers ruptured firstly in the stretching process, then the loading-force on PAN fibers increased rapidly. The thickness of BP layer increased, and higher concentrated stress would load on PAN fibers after BP layer rupturing. Then PAN fibers also ruptured faster. Therefore, CNT areal density increasing also provided a negative effect on the elongation at break of composite films. In addition, both the average tensile strength and elongation at break of 3#BP/PAN film (19.99 Mpa, 7.1%) were lower than PAN mat (29.19 MPa, 38.65%), but those were higher than 3#BP (17.91 MPa, 0.83%), according to the bucket effect of composite. The improvement of mechanical properties of composite film was attributed to the interface reinforcement between CNTs and PAN fibers and higher mechanical properties of PAN fibers.

3.3. Electrical property analysis

Materials with excellent electrical conductivities usually possess high EMI shielding abilities. Thus, electrical conductivity is a significant property for EMI shielding material. Because the microwave reflection was mainly depended on conduction paths of electrons [42]. Both the average slice resistivities and conductivities of BP layers of 1-4#BP/PAN composite films were presented in Table 1. Thereinto, the average conductivity had been calculated according to the average slice resistivity. Conductivity values of BP/PAN composite films increased rapidly first. When the CNT areal density was equal or greater than 3 mg/cm^2, the conductivities fluctuated around a constant value of ~527.1 S/cm. The reason was that electric current only flowed through the outer tubes of CNT bundles, and the junction resistance mainly

Table 1
The average slice resistivity and electrical conductivities of pristine PAN mat, 3#BP and 1-4#BP/PAN composites contrast with the references.

Samples	Slice Resistivity (mΩ·cm)	Conductivity (S/cm)
1#BP/PAN	11.08 ± 0.2	90.33 ± 1.66
2#BP/PAN	3.81 ± 0.1	262.47 ± 7.07
3#BP/PAN	1.90 ± 0.16	527.10 ± 44.33
4#BP/PAN	1.90 ± 0.16	527.10 ± 44.33
3# BP	1.76 ± 0.1	568.18 ± 34.22
Pristine-PAN	–	Insulation
SWCNT	0.1	1×10^4
CNT/PAN Composite	3.47×10^4	2.886×10^{-2}

came from tube-tube contact and intra-bundle juncture of CNT bundles. The junction resistance between CNT bundles almost dominated the overall electrical transport, since the electron path of inner of CNT that contributed little to current flowing through could be neglected [43]. CNT content played an important role in enhancement of electrical conductivity for BP/PAN composite before the CNT areal density was less than 3 mg/cm^2. However, the average slice resistivity and conductivity of BP layer of 3#BP/PAN were similar to 3#BP, and its conductivity was much higher than CNT/PAN composite [44]. It meant that conductive paths for electrons in BP layer of BP/PAN composite were not impeded by the introduction of PAN fibers.

3.4. Electromagnetic interference shielding property analysis

It is well known that EMI shielding ability of material can be characterized in terms of shielding effectiveness (SE) that is the logarithmic ratio of incoming (P_I) to transmitted (P_T) power of microwaves [45]. The electromagnetic waves shoot on the surface of CNT/PAN layer of BP/PAN composite film, then three types of phenomena will be observed, namely, reflection (SE_R), absorption (SE_A) and multiple reflection (SE_M) [46]. Therefore, the sum of all these phenomena is total EMI shielding effectiveness (SE_{total}) that could be expressed as [47]

$$SE_{total}(dB) = SE_R + SE_A + SE_M = 10\log(P_I/P_T) \quad (1)$$

When $SE_{total} > 15$ dB, SE_M can be neglected [9,10,48]. Thus, the SE_{total} can be written in simplification mode as [49]

$$SE_{total}(dB) = SE_R + SE_A \quad (2)$$

All the SE_R and SE_{total} of PAN mat, 3#BP and 1-4#BP/PAN composite films were recorded with VNA and waveguide tube in Fig. 7(a). Moreover, the SE_{total}, and SE_R of BP/PAN composite films were measured through incident wave shooting on the CNT/PAN layers, due to the direction of incident wave severely affecting their shielding effectiveness. According to Eq. (2), SE_A values of 3#BP and 1-4#BP/PAN composite films were gotten by calculation. The PAN mat was an insulating material, thus, its SE_{total} was too low and not necessary to discuss.

Fig. 7(b)–(d) presented the variation of SE_{total}, SE_R and SE_A values of 1-4#BP/PAN composite films and 3#BP in the Ku band (12 to 18 GHz), respectively. The SE_{total} of PAN electrospun film was less than 1.5 dB, thus its SE_{total}, SE_R and SE_A curves were not displayed in Fig. 7(b)–(d). From Fig. 7(c)–(d), all of SE_R of composites was higher than SE_A. Moreover, SE_R value ranges of 1-4#BP/PAN film showed a slowly ascending trend with CNT areal density increasing, due to conductivity increasing. SE_R value range of 1#BP/PAN film was the lowest (30–38.9 dB) and that of 4#BP/PAN composite was the highest (33.9–43.5 dB). SE_R value range of 4#BP/PAN film was higher than 3#BP/PAN (33.5–42.7 dB), because thickness of 4#BP/PAN was higher than 3#BP/PAN film. Thus, SE_R of BP/PAN composite film related to conductivity and thickness [50,51]. However, SE_A values of BP/PAN composite films exhibited the first increasing and then decreasing trend. The reason was the CNTs permeating into PAN mat could form

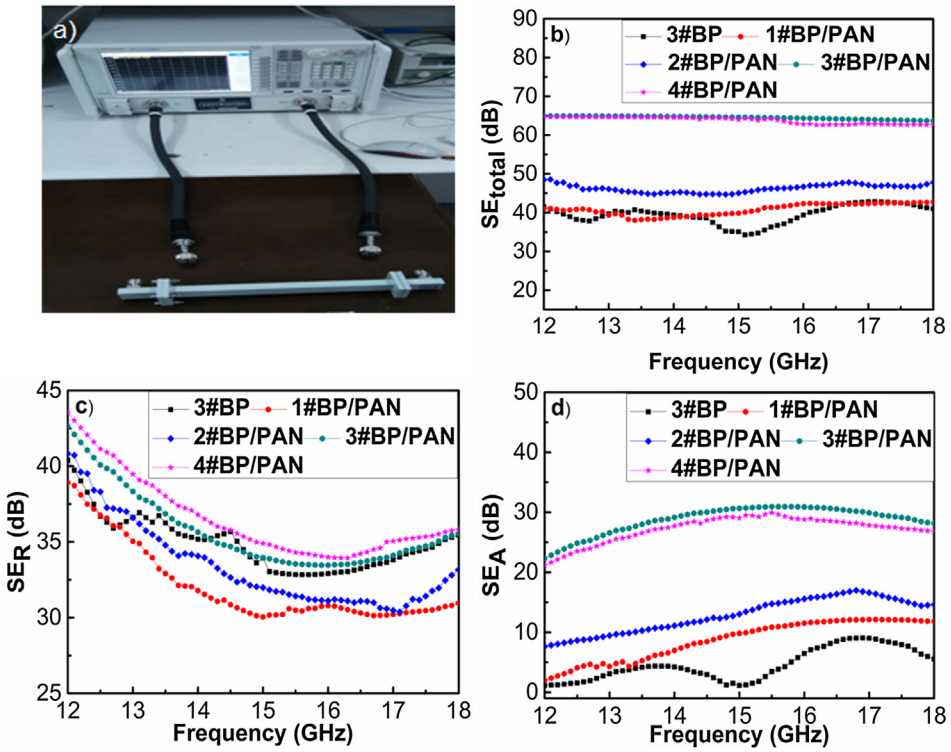

Fig. 7. (a) VNA and waveguide tube, (b) Total SE, (c) SE reflection, and (d) SE absorption of 1-4#BP/PAN composite films and 3#BP in 12–18 GHz. (For interpretation of the references to colour in this figure legend, the reader is referred to the web version of this article.)

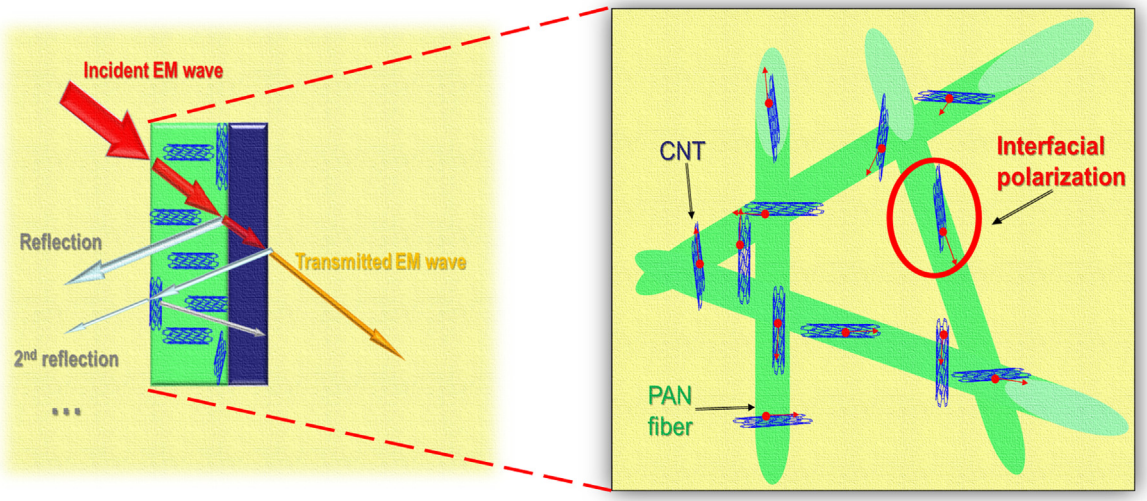

Fig. 8. The schematic representation of EMI shielding mechanism in BP/PAN composite film. (For interpretation of the references to colour in this figure legend, the reader is referred to the web version of this article.)

interfaces between CNTs and PAN fibers. Before the CNT areal density reaching the extreme value, more CNTs permeating into PAN mat could consume more electromagnetic wave power. Thus, SE_A range of 3#BP/PAN composite was the maximum (22.3–31 dB) and the minimum value range belonged to 1#BP/PAN (2–12.1 dB). When the CNT quantity in CNT/PAN layer increased over the extreme value, the CNTs formed some small conductive networks in CNT/PAN layer. The small conductive networks made the reflection ability of CNT/PAN layer increasing, but the absorbing ability decreasing [52–54]. It was equal to construct many barriers for electromagnetic wave. Chances of electromagnetic wave consumption reducing led the SE_A of CNT/PAN layer descending. For instance, SE_A range of 4#BP/PAN film that was ranged from 21.2 to 29.9 dB was lower than 3#BP/PAN (22.3–31 dB). Meanwhile, SE_{total} values of BP/PAN composite films also showed the same trend as their SE_A. SE_{total} value range of 1#BP/PAN film was the minimum (38–42.8 dB) in four composite films, and that of 3#BP/PAN film was the maximum (63.7–65 dB). From the above descriptions, reflection abilities of BP/PAN composites changed little with variation of CNT content, while the CNT quantity in CNT/PAN layer had direct influence on absorbing abilities of composite films. Additionally, the SE_{total}, SE_A and SE_R of 3#BP and 3#BP/PAN were compared in Fig. 7(b)–(d). SE_A value range of 3#BP/PAN film was higher than 3#BP (1.1–9.1 dB), because its CNT/PAN layer contained massive interfaces that could consume microwave energy. Furthermore, SE_R values of

3#BP (32.8–40.4 dB) and 3#BP/PAN film displayed little difference. Therefore, SE_{total} values of 3#BP/PAN composite film were much higher than 3#BP (34.3–42.9 dB). It proved that the CNT/PAN layer as an absorbing layer played a major role in improving the SE_{total} of BP/PAN film. When incident wave shot on the CNT/PAN layers, the EMI shielding mechanism of BP/PAN composite film was displayed through a schematic diagram in Fig. 8.

All the SE_{total} of 1-4#BP/PAN composites exceeded 38 dB, which met the EMI shielding requirements for applications in engineering. Compared with the data reported in references, it was noted that the BP/PAN composite film with better flexibility and high EMI shielding effectiveness was more competitive than other polymer or carbon matrix EMI shielding composites in Ku band. For example, the SE_{total} of MWCNTs/PF [55] composite paper was only 32.4 dB and that of MWCNT-g-Fe_3O_4 in PC/SAN blends [56] was 32.5 dB, etc [57].

4. Conclusions

This work provided a facile preparation strategy of BP/PAN composite film with better flexibility and higher EMI shielding performance. The mechanical properties of 3#BP/PAN composite film were enhanced markedly through interface reinforcing and the introduction of PAN fibers. Its tensile strength and elongation at break were improved about 12% and 761%, compared with buckypaper having the same areal density (3#BP). Meanwhile, the 3#BP/PAN composite also exhibited excellent electrical conductivity (527.1 S/cm) as 3#BP. However, 3#BP/PAN film possessed higher SE_{total} (65 dB) than 3#BP (42.9 dB) and it could meet the EMI shielding requirements for applications in engineering. Considering the mechanical and EMI shielding properties of 1-4#BP/PAN films, the 3#BP/PAN composite film possessed the better overall performance. As a novel EMI shielding material, 3#BP/PAN composite film with excellent performance would become a candidate for the military and civil applications, such as flexible antenna, EMI shielding tent, EMI shielding clothes and soft portable electronic products.

Acknowledgements

This work is supported by the National Natural Science Foundation of China [Grant Nos. 11225211, 11272106]. Project supported by the Foundation for Innovative Research Groups of the National Natural Science Foundation of China [Grant No. 11421091].

References

[1] Choi HY, Lee TW, Lee SE, Lim JD, Jeong YG. Silver nanowire/carbon nanotube/cellulose hybrid papers for electrically conductive and electromagnetic interference shielding elements. Compos Sci Technol 2017;150:45–53.
[2] Chaudhary A, Kumari S, Kumar R, Teotia S, Singh BP, Singh AP, et al. Lightweight and easily foldable MCMB-MWCNTs composite paper with exceptional electromagnetic interference shielding. ACS Appl Mater Inter 2016;8:10600–8.
[3] Gargama H, Thakur AK, Chaturvedi SK. Polyvinylidene fluoride/nanocrystalline iron composite materials for EMI shielding and absorption applications. J Alloy Compd 2016;654:209–15.
[4] Andrés JA, González NP, Fonseca C, Pérez E, Cerrada ML. Lightweight nanocomposites based on poly(vinylidene fluoride) and Al nanoparticles: structural, thermal and mechanical characterization and EMI shielding capability. Mat Chem Phys 2013;142:469–78.
[5] Zhao H, Hou L, Lu YX. Electromagnetic shielding effectiveness and serviceability of the multilayer structured cuprammonium fabric/polypyrrole/copper (CF/PPy/Cu) composite. Chem Eng J 2016;297:170–9.
[6] Gass J, Poddar P, Almand J, Srinath S, Srikanth H. Superparamagnetic polymer nanocomposites with uniform Fe_3O_4 nanoparticle dispersions. Adv Funct Mater 2006;16:71–5.
[7] Singh R, Kulkarni GS. Nanocomposites based on transition metal oxides in polyvinyl alcohol for EMI shielding application. Polym Bull 2014;71:497–513.
[8] Gupta A, Singh AP, Varshney S, Agrawal N, Sambyal P, Pandey Y, et al. New insight into the shape-controlled synthesis and microwave shielding properties of iron oxide covered with reduced graphene oxide. RSC Adv 2014;4:62413–22.
[9] Hsiao ST, Ma MC, Liao WH, Wang YS, Li SM, Huang YC, et al. Lightweight and flexible reduced graphene oxide/water-borne polyurethane composites with high electrical conductivity and excellent electromagnetic interference shielding performance. ACS Appl Mater Inter 2014;6:10667–78.
[10] Hu MJ, Gao JF, Dong Y, Li K, Shan G, Yang S, et al. Flexible transparent PES/silver nanowires/PET sandwich-structured film for high-efficiency electromagnetic interference shielding. Langmuir 2012;28:7101–6.
[11] Mapkar JA, Belashi A, Berhan LM, Coleman MR. Formation of high loading flexible carbon nanofiber network composites. Compos Sci Technol 2013;75:1–6.
[12] Hong MS, Choi WK, An KH, Kang SJ, Park SJ, Lee YS, et al. Electromagnetic interference shielding behaviors of carbon fibers-reinforced polypropylene matrix composites: II. Effects of filler length control. J Ind Eng Chem 2014;20:3901–4.
[13] Guo Y, Xu G, Yang X, Ruan K, Ma T, Zhang Q, et al. Significantly enhanced and precisely modeled thermal conductivity in polyimide nanocomposites with chemically modified graphene via in situ polymerization and electrospinning-hot press technology. J Mater Chem C 2018;6:3004–15.
[14] Gu J, Yang X, Lv Z, Li N, Liang C, Zhang Q. Functionalized graphite nanoplatelets/epoxy resin nanocomposites with high thermal conductivity. Int J Heat Mass Transfer 2016;92:15–22.
[15] Gu J, Li N, Tian L, Lv Z, Zhang Q. High thermal conductivity graphite nanoplatelet/UHMWPE nanocomposites. RSC Adv 2015;5:36334–9.
[16] Fakirov S, Rahman MZ, Potschke P, Bhattacharyya D. Single polymer composites of poly(butylene terephthalate) microfibrils loaded with carbon nanotubes exhibiting electrical conductivity and improved mechanical properties. Macromol Mater Eng 2013:1–8.
[17] Zeng Z, Jin H, Chen M, Li W, Zhou L, Zhang Z. Lightweight and anisotropic porous MWCNT/WPU composites for ultrahigh performance electromagnetic interference shielding. Adv Funct Mater 2016;26:303–10.
[18] Yang X, Liang C, Ma T, Guo Y, Kong J, Gu J, et al. A review on thermally conductive polymeric composites: classification, measurement, model and equations, mechanism and fabrication methods. Adv Compos Hybrid Mater 2018:1–24.
[19] Iijima S. Helical microtubules of graphitic carbon. Nature 1991;354:56–8.
[20] Falzon BG, Robinson P, Frenz S, Gilbert B. Development and evaluation of a novel integrated anti-icing/de-icing technology for carbon fibre composite aerostructures using an electro-conductive textile. Compos Part A-Appl S 2015;68:323–35.
[21] Xing H, Sun L, Song G, Gou J, Hao YW. Surface coating of carbon nanofibers/nanotubes by electrodeposition for multifunctionalization. Nanotechnology 2008;19:025704.
[22] Han J, Zhang H, Chen M, Wang D, Liu Q, Wu Q, et al. The combination of carbon nanotube buckypaper and insulating adhesive for lightning strike protection of the carbon fiber/epoxy laminates. Carbon 2015;94:101–13.
[23] Ryu S, Kim BG, Choi JW, Lee H. Highly oriented carbon nanotube sheets for rechargeable lithium oxygen battery electrodes. J Nanosci Nanotechno 2015;15:7611–4.
[24] Jin Y, Chen H, Chen M, Liu N, Li Q. Graphene-patched CNT/MnO_2 nanocomposite papers for the electrode of high-performance flexible asymmetric supercapacitors. ACS Appl Mater Inter 2013;5:3408–16.
[25] Villalpando PF, Moura LG, Fantini C, Muramatsu H, Hayashi T, Kim YA, et al. Tunable raman spectroscopy study of CVD and peapod-derived bundled and individual double-wall carbon nanotubes. Phys Rev B 2010;82:155416.
[26] Lu HB, Lei M, Leng JS. Significantly improving electro-activated shape recovery performance of shape memory nanocomposite by self-assembled carbon nanofiber and hexagonal boron nitride. J Appl Poly Sci 2014:40506.
[27] Zhang J, Jiang D, Peng HX, Qin F. Enhanced mechanical and electrical properties of carbon nanotube buckypaper by in situ cross-linking. Carbon 2013;63:125–32.
[28] Liu Q, Li M, Wang Z, Gu Y, Li Y, Zhang Z. Improvement on the tensile performance of buckypaper using a novel dispersant and functionalized carbon nanotubes. Compos Part A-Appl S 2013;55:102–9.
[29] Chou TW, Gao L, Thostenson ET, Zhang Z, Byun JH. An assessment of the science and technology of carbon nanotube-based fibers and composites. Compos Sci Technol 2010;70:1–19.
[30] Zhang Z, Zhang F, Jiang X, Liu Y, Guo Z, Leng J. Electrospinning and microwave absorption of polyaniline/polyacrylonitrile/multiwalled carbon nanotubes nanocomposite fibers. Fiber Polym 2014;15(11):2290–6.
[31] El-Newehy HM, Al-Deyab SS, Kenawy ER, Abdel-Megeed A. Nanospider technology for the production of nylon-6 nanofibers for biomedical applications. J Nanomater 2011:626589.
[32] Chu HT, Zhang ZC, Liu YJ, Leng JS. Silver particles modified carbon nanotube paper/glassfiber reinforced polymer composite material for high temperature infrared stealth camouflage. Carbon 2016;98:557–66.
[33] Gu J, Dong W, Xu S, Tang Y, Ye L, Kong J. Development of wave-transparent, lightweight composites combined with superior dielectric performance and desirable thermal stabilities. Compos Sci Technol 2017;144:185–92.
[34] Chung DDL. Electromagnetic interference shielding effectiveness of carbon materials. Carbon 2001;39:279–85.
[35] Yousefi N, Sun X, Lin X, Shen X, Jia J, Zhang B, et al. Highly aligned graphene/polymer nanocomposites with excellent dielectric properties for high-performance electromagnetic interference shielding. Adv Mater 2014;26:5480–7.
[36] Zeng Z, Chen M, Pei Y, Shahabadi SIS, Che B, Wang P, et al. Ultralight and flexible polyurethane/silver nanowire nanocomposites with unidirectional pores for highly effective electromagnetic shielding. ACS Appl Mater Interfaces 2017;9:32211–9.
[37] Zeng Z, Wang C, Zhang Y, Wang P, Shahabadi SIS, Pei Y, et al. Ultralight and highly elastic graphene/lignin-derived carbon nanocomposite aerogels with ultrahigh electromagnetic interference shielding performance. ACS Appl Mater Interfaces 2018;10:8205–13.
[38] Zeng Z, Jin H, Chen M, Li W, Zhou L, Xue X, et al. Microstructure design of lightweight, flexible, and high electromagnetic shielding porous multiwalled carbon nanotube/polymer composites. Small 2017;13:1701388.
[39] Masanori I, Kousuke A, Tomo T, Eiichi S. Highly strong and conductive carbon

nanotube/cellulose composite paper. Compos Sci Technol 2010;70:1564–70.
[40] Hayashida K, Matsuoka Y. Electromagnetic interference shielding properties of polymer-grafted carbon nanotube composites with high electrical resistance. Carbon 2015;85:363–71.
[41] Hu H, Lu X, Wang F, He J, Li J, Fan M. Activated carbon based selective purification of medical grade NO starting from arc discharge method. Carbon 2011;49:2197–205.
[42] Li N, Huang Y, Du F, He X, Lin X, Gao H, et al. Electromagnetic interference (EMI) shielding of single-walled carbon nanotube epoxy composites. Nano Lett 2006;6(6):1141–5.
[43] Kaiser AB, Skakalova V. Electronic conduction in polymers, carbon nanotubes and graphene. Chem Soc Rev 2011;40(7):3786–801.
[44] Han SJ, Kim B, Suh KD. Electrical properties of a composite film of poly(acrylonitrile) nanoparticles coated with carbon nanotubes. Macromol Chem Phys 2007;208:377–83.
[45] Zhang X, Zhang X, Yang M, Yang S, Wu H, Guo S, et al. Ordered multilayer film of (graphene oxide/polymer and boron nitride/polymer) nanocomposites: An ideal EMI shielding material with excellent electrical insulation and high thermal conductivity. Compos Sci Technol 2016;136:104–10.
[46] Lee TW, Lee SE, Jeong YG. Carbon nanotube/cellulose papers with high performance in electric heating and electromagnetic interference shielding. Compos Sci Technol 2016;131:77–87.
[47] Gupta T, Singh B, Teotia S, Katyal V, Dhakate S, Mathur R. Designing of multiwalled carbon nanotubes reinforced polyurethane composites as electromagnetic interference shielding materials. J Polym Res 2013;20(6):1–7.
[48] Yuan B, Yu L, Sheng L, An K, Zhao X. Comparison of electromagnetic interference shielding properties between single-wall carbon nanotube and graphene sheet/polyaniline composites. J Phys D: Appl Phys 2012;45:235108.
[49] Park JG, Louis J, Cheng Q, Bao J, Smithyman J, Liang R, et al. Electromagnetic interference shielding properties of carbon nanotube buckypaper composites. Nanotechnology 2009;3(20):415702.
[50] Zeng Z, Chen M, Jin H, Li W, Xue X, Zhou L, et al. Thin and flexible multi-walled carbon nanotube/waterborne polyurethane composites with high-performance electromagnetic interference shielding. Carbon 2016;96:768–77.
[51] Shahzad F, Alhabeb M, Hatter CB, Anasori B, Hong SM, Koo CM, et al. Electromagnetic interference shielding with 2D transition metal carbides (MXenes). Science 2016;353(6304):1137–40.
[52] Kumar A, Singh AP, Kumari S, Srivastava AK, Bathula S, Dhawan SK, et al. EM shielding effectiveness of Pd-CNT-Cu nanocomposite buckypaper. J Mater Chem A 2015;3:13986–93.
[53] Komarov FF, Zukowski P, Kryvasheyeu RM, Munoz E, Koltunowicz TN, Rodionova VN, et al. Effects of surfactant and fabrication procedure on the electrical conductivity and electromagnetic shielding of single-walled carbon nanotube films. Phys Status Solidi A 2015;2:425–32.
[54] Fugetsu B, Sano E, Sunada M, Sambongi Y, Shibuya T, Wang X, et al. Electrical conductivity and electromagnetic interference shielding efficiency of carbon nanotube/cellulose composite paper. Carbon 2008;46(9):1256–8.
[55] Teotia S, Singh BP, Elizabeth I, Singh VN, Ravikumar R, Singh AP, et al. Multifunctional, robust, light-weight, free-standing MWCNT/phenolic composite paper as anodes for lithium ion batteries and EMI shielding material. RSC Adv 2014;4(63):33168–74.
[56] Pawar PS, Marathe AD, Pattabhi K, Bose S. Electromagnetic interference shielding through MWNT grafted Fe_3O_4 nanoparticles in PC/SAN blends. J Mater Chem A 2015;3:656–69.
[57] Verma P, Saini P, Malik RS, Choudhary V. Excellent electromagnetic interference shielding and mechanical properties of high loading carbon nanotubes/polymer composites designed using melt recirculation equipped twin-screw extruder. Carbon 2015;89:308–17.